Journal of Solar Energy Research (JSER)

Journal homepage: www.jser.ut.ac.ir

Optimal Demand Response-Based AC OPF Over Smart Grid Platform Considering Solar and Wind Power Plants and ESSs with Short-Term Load Forecasts Using LSTM

Alireza Zarei[a], Navid Ghaffarzadeh[a,*]

[a]Department of Electrical Engineering, Faculty of Technical and Engineering, Imam Khomeini International University, Qazvin, Iran

Received: 16-12-2022
Accepted: 09-02-2023

Abstract

By adding renewable energy sources, such as solar and wind, advanced metering infrastructure, and energy storage systems, the traditional power grid is becoming a smart grid. To prevent the uneconomic operation of a smart grid and increase the penetration of renewable resources, the Demand Response (DR) method is crucial for reducing the peak load and passing critical conditions. In this context, this study presents a multi-objective optimization of the AC optimal power flow (AC-OPF) problem with respect to DR. The novelty of the proposed demand-response-based OPF approach consists of decreasing the system cost through the simultaneous participation of active and reactive power in DR, considering the physical constraints of the AC network and various renewable energy sources in the smart grid, and increasing the calculation accuracy by demand prediction based on previous data using deep learning methods. Finally, using the TOPSIS method, the best DR value was determined according to multi-objective optimization. The effectiveness and resiliency of the proposed method were validated using a modified IEEE 24-bus testing system. The results illustrate that the optimal demand response (20%) achieved not only peak reduction and valley filling in active and reactive power but also minimized the total voltage deviation and system cost.

Keywords: Solar power plant; Demand response; Optimal power flow; Renewable energy; Load forecasting; Smart grid

DOI: 10.22059/jser.2023.352567.1271 DOR: 20.1001.1.25883097.2023.8.2.2.0

1. Introduction

In the last few years, the conventional power grid has been redesigned into a smart, highly efficient, and fully integrated system, the so-called smart grid (SG). Conventional electricity consumers have become prosumers who can produce and consume electricity with the development of Distributed Energy Resources (DERs) such as Photovoltaics (PV), Energy Storage Systems (ESS), Electric Vehicles (EV) [1], smart meters, and future electricity needs [2]. Only three renewable energy sources (biomass, geothermal, and solar) can be used to generate sufficient heat energy for power generation [3]. Of these, solar energy exhibits the highest global potential because geothermal sources are limited to a few locations, and the supply of biomass is not ubiquitous in nature [4]. In addition,

*Corresponding Author Email Address: ghaffarzadeh@eng.ikiu.ac.ir

noise effects near populated areas [5], low robustness, narrow wind speed range, and low output power of current small-scale wind energy harvesters [6] are disadvantages of wind energy. During the last decade, a significant decrease in the price of renewable energy sources, where the cost of PV has decreased by 90% [7], has led to more use of solar energy. Mbachu et al. [8] conducted an economic analysis and comparison between a solar photovoltaic system and fossil fuel-powered electricity generators in the Awka University campus, and the results showed that optimization (minimization) of the electricity load reduced the initial acquisition and installation cost of the solar photovoltaic system, which is more economical than fossil fuel-powered electricity generators. Solar energy is an abundant renewable energy source that can provide energy with high security values. This energy source is freely available in many regions of the world, especially in the Middle East and North Africa [9].

Demand side management (DSM) is an important function in a smart grid that allows customers to make informed decisions regarding their energy consumption and helps energy providers reduce the peak load demand and reshape the load profile [10]. DSM methods can be classified into energy response (energy efficiency and conservation (EEC)) and demand response (DR) [11]. Demand Response (DR) is considered the most cost-effective and reliable solution for smoothing the demand curve when the system is under stress [12]. Generally, the peak load of the electricity network occurs during the hot months of the year owing to the operation of cooling systems. The increased demand for electricity may require an uneconomical ramp-up of expensive generators, resulting in increased real-time electricity prices, which can be as high as 100 times the average value. In such cases, load-serving entities (LSE) who buy energy in the wholesale power market and dispatch it to residential (or commercial) consumers may have to procure energy at very high prices [13]. To prevent the uneconomic operation of the power grid, the Demand Response (DR) method was used to reduce the peak load and pass critical conditions. In addition, the need to build expensive new power plants has been eliminated or delayed. It can be expected that demand response will be an important stepping stone toward the practical deployment of smart grids [14]. DR options are generally categorized into price-based demand response (PBDR) and incentive-based demand response (IBDR) programs [15]. As described in Figure 1, All the PBDR programs are voluntary; however, the IBDR programs include voluntary programs, mandatory programs, and market clearing programs [16]. Along with DR methods, the load shedding method is also mentioned; for example, Ahmadipour et al. [17] proposed an optimal load shedding method using an optimization algorithm to maintain the stability of an islanded power system that comprises distributed energy resources (DER). In addition, under emergency conditions, load shedding is considered the most effective approach to maintain the power balance and stability; however, the DR methods are more favorable than the load shedding method because in the DR, only the time of load consumption is shifted, but in load shedding, a part of the load must be interrupted.

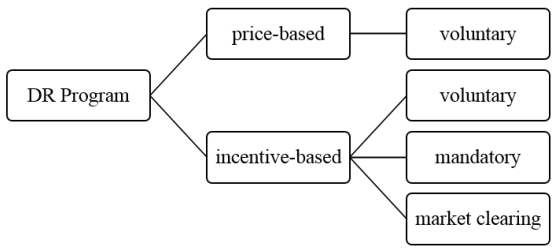

Figure 1. Demand response categories

The AC Optimal Power Flow (AC-OPF) is a nonconvex optimization problem, where the objective is to minimize the cost of generation subject to power balance constraints described by Kirchhoff's current and voltage laws and operational constraints reflecting real and reactive limits on power generation, bus voltage magnitudes, and power flows along transmission lines [18]. The nonconvexity of the OPF problem is due to the quadratic equations of the AC network. The treatment of such non-convexities in ACOPF has traditionally relied on the use of local constrained optimization methods, or convex relaxation and linear approximation methods [19], where DC Power Flow denotes the linearization form of the original AC Power Flow equations. Compared to the DC-OPF formulation, the benefits of the AC Optimal Power flow (AC-OPF) are (i) increased accuracy, (ii) considered voltage, (iii) considered reactive power, (iv) considered currents, and (v) considered transmission losses [20]. The linear optimal power flow (LOPF) method is more suitable than the DCOPF in the distribution network because the problem of a lack of voltage range and subsequently reactive power in the DCOPF has been solved. In addition, LOPF models are

computationally inexpensive, but their solutions fail to satisfy AC power flow constraints [21]. The results obtained using the AC-OPF were more accurate [22].

In smart grids and microgrids, different objective functions (OFs), such as active power generation cost, reactive power generation cost, power supplied to the grid from an external utility, active power losses, carbon emissions, load curtailment, tap position and capacitor bank switching, social welfare, reserve cost, and load adjustment, are considered in the optimal power flow (OPF) [22]. Few studies have been conducted on demand response (DR) based on AC optimal power flow (OPF) analysis. Jabari et al. [23] present the integration of the AC optimal power flow (AC-OPF) problem with demand response programs (DRPs). A time-value-based demand-shifting strategy was used to reduce the peak load and shift this value to other mid- and low-demand hours. In this method, the effect of reactive power changes in the DR is not considered. Haggi et al. [24] proposed DR modeling in Active Distribution Networks (ADN) by considering both active and reactive power shifting while preserving the power factor of each load. Shi et al. [25] investigated the joint coordination of demand response and AC optimal power flow with curtailment of renewable energy resources. An ADMM-based DMPC algorithm was used to predict the future power demand. Yao et al. [26] proposed a multiperiod optimal power flow (OPF) approach that uses DR to improve steady-state voltage stability to improve voltage stability in transmission networks. Both [25] and [26] have complicated execution methods, and their execution times are long. To mitigate the overvoltage over network buses in high-power systems with high PV-penetrated penetration, Heidari Yazdi et al. [27] proposed an active power curtailment (APC) and reactive power control method applied to buses with PV inverters. The demand response (DR) program is employed using load-shifting techniques to move a portion of the load from peak hours. This method is only applicable to buses with PV and to prevent overvoltage, and it is not considered a comprehensive method to be implemented for the entire smart grid. Merrad et al. [28] proposed a fully decentralized architecture for an OPF-based demand response management system by mathematical modelling that uses smart contracts to force generators to comply without the need for a central authority. However, the execution cost is related to the number of provers participating in the smart contract, because of the requirement to loop the smart contract through all provers.

The main contributions of this paper can be summarized as follows: (1) an Optimal Demand Response-based OPF formulation is proposed for total cost reduction and peak shaving in the smart grid ; (2) to increase the accuracy of future electrical load prediction using previous consumption data, the LSTM method is used; (3) the proposed problem consists of various types of generating power units and ESS; (4) in addition to active power, reactive power is also considered in the proposed demand response program; (5) to compare the various cases of demand response problems and select the optimal point TOPSIS method used.

The remainder of this paper is organized as follows: Section 2 presents methodology containing Description of the problem, demand prediction, the problem formulation and demand response program. Section 3 analyzes the case studies and data. Section 4 reports the simulation results for the modified IEEE 24-bus test system. Finally, the main conclusions of this study are presented in section 5.

2. Methodology

2.1 Description of the problem

The aim of the DR-OPF problem is to optimize the objective functions while simultaneously satisfying a set of equality and inequality constraints at the same time by considering the DR. In this problem, the electrical load predicted by the LSTM method and schematic solar/wind power generation were added as inputs to the optimization problem. The optimization problem is solved in various steps of DR. Subsequently, the objective functions of the aforementioned steps are compared to select the best operation point.

2.2. Demand prediction

Demand forecasting is an essential factor in the operation and planning of energy production and distribution systems. If the energy consumption is overestimated, idle production capacity is designed, and the consumption cost of all subscribers will increase without a valid reason. However, underestimating energy consumption has negative economic and social impacts such as blackouts and brownouts [29]. Electrical Energy Demand (EED) forecasting techniques can be clustered into three (3), namely correlation, extrapolation, and a combination of both [30]. Different load forecasting

models can be broadly classified into engineering methods (correlation) and data-driven methods (extrapolation or Artificial Intelligence) [31]. In engineering methods, parameters, such as temperature and weather, are used to calculate the amount of energy consumed. However, in data-driven methods, the load consumption information from previous periods is used to predict future consumption.

Machine learning is a subsection of Artificial Intelligence (AI) that imparts the system; the benefits of automatically learning from concepts and knowledge without being explicitly programmed [32]. Depending on how an algorithm is being trained and based on the availability of the output during training, machine learning paradigms can be classified into ten categories [33], and the artificial neural network (ANN) is one of these categories. In an artificial neural network (ANN) system, the amount of information is increased using learning algorithms, and as a result, the efficiency of the educational process is improved. This process is called deep learning because the number of layers of the neural network increases over time. Owing to the greater number of layers, machine learning is also known by other titles such as deep structured learning and hierarchical learning. The deep learning method was performed in two modes: supervised and unsupervised.

To forecast the electrical demand, hourly data for one month (from August 19 to September 19, 2022) for New Zealand [34], including active and reactive power, were used. The deep neural network architecture is of the long short-term memory (LSTM) type, which is suitable for predicting time series. MATLAB software was used to implement the LSTM problem. In this problem, 90% and 10% of the information is used for training and test data, respectively. The Training option settings including 'MaxEpochs,' 'GradientThreshold,' 'InitialLearnRate,' 'LearnRateDropPeriod,' and 'LearnRateDropFactor' are set to 250, 1, 0.005, 125, and 0.2, respectively. After training the deep neural network and improving the predictions, the state of the network was updated using real values. The normal and improved modes of the LSTM deep learning are shown in Figures 2 and 3, respectively.

The root-mean-square error (RMSE) and mean absolute error (MAE) were used to evaluate the load prediction performance. The values of RMSE and MAE in the normal mode, were 398.1 and 292.5, respectively, and those in the improved mode were 57 and 292.5, respectively. It can be seen that the correlation between the predicted and observed values increased significantly after updating the deep neural network, and the root mean square error (RMSE) value decreased significantly. For simplicity, a 24-hour load forecast was applied to all the load buses.

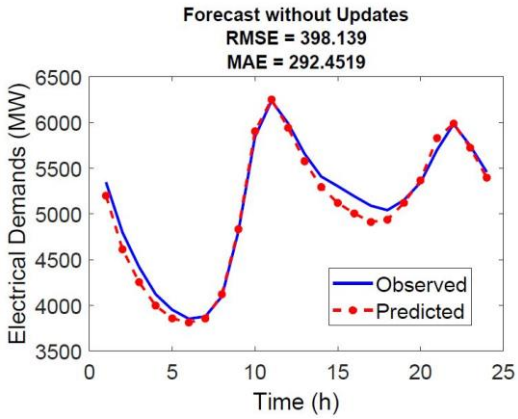

Figure 2. Normal LSTM load prediction

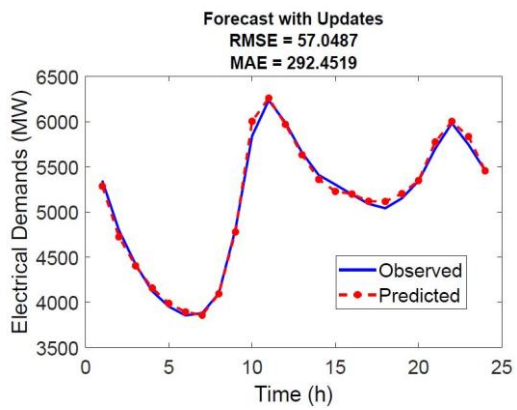

Figure 3. Modified LSTM load prediction

2.3. Problem formulation

The objective functions of the problem and its constraints are as follows:

A. Objective Functions

1) Cost Function

The cost function consists of active and reactive generation costs, the cost of load shedding, and the wind/solar curtailment cost [35], [36].

$$OF_1 = b_g P_{i,t}^{g} + c_g Q_{i,t}^{g} + \sum_{i,t} VOLL \times P_{i,t}^{LS} + \sum_{i,t} VOLW \times P_{i,t}^{WC} + \sum_{i,t} VOLS \times P_{i,t}^{SC} \quad (1)$$

where b_g, c_g, $P_{i,t}^{g}$, $P_{i,t}^{LS}$, $P_{i,t}^{WC}$, and $P_{i,t}^{SC}$ are the fuel cost coefficients of active power generation at unit g,

reactive power generation at unit g, power generation of unit i at time t, Active Load shedding in bus i at time t, and wind and solar curtailment in bus i at time t, respectively. In the objective function, the quadratic cost of the power plants is approximated using a first-order function. VOLL is the value of load loss according to the graph of wind and demand changes, which is considered a penalty. Similarly, VOLW/VOLS is the cost factor for reducing wind/solar energy production in wind/solar power plants according to the graph of wind/solar and demand changes. According to [36] and [37], nodal reactive power pricing is another way to design a price structure. This is the sensitivity of the generation production cost to the reactive power demand and is usually computed by the OPF. The cost of reactive power is approximately one percent of the cost of active power. Therefore, in the objective function, one percent of the active power production cost coefficient is applied as a coefficient related to reactive power generation cg=0.01bg.

2) Voltage Deviation Function (VDF) [38]

$$OF_2 = \sum_{i,t} \left| V_{slack} - V_i \right| \tag{2}$$

where the voltage deviation function is applied to improve the voltage profile and power quality, V_i is the voltage at bus i, and V_{slack} is equal to one in this study.

$$OF_3 = \frac{P_{load}^{new} - P_{load}^{old}}{P_{load}^{old}} \times 100 \tag{3}$$

This objective function calculates the amount of peak load reduction after demand response compared to the normal state as a percentage.

B. Active and Reactive Power Relationships

The active and reactive power relationships in the AC network are as follows [40]:

$$P_{ij,t} = \mathrm{Re}\left\{S_{ij,t}\right\} = \frac{V_{i,t}^2}{Z_{ij}} \cos\left(\theta_{ij}\right) - \frac{V_{i,t}V_{\mathrm{j},t}}{Z_{ij}} \cos\left(\delta_{i,t} - \delta_{\mathrm{j},t} + \theta_{ij}\right) \tag{4}$$

$$Q_{ij,t} = \mathrm{Im}\left\{S_{ij,t}\right\} = \frac{V_{i,t}^2}{Z_{ij}} \sin\left(\theta_{ij}\right) - \frac{V_{i,t}V_{\mathrm{j},t}}{Z_{ij}} \sin\left(\delta_{i,t} - \delta_{\mathrm{j},t} + \theta_{ij}\right) - \frac{bV_{i,t}^2}{2} \tag{5}$$

C. Power Balance Constraints

At time step t, the balance of the active and reactive power in all buses is given by.

$$P_{i,t}^g + P_{i,t}^{LS} + P_{i,t}^W + P_{i,t}^S + \left(-P_{i,t}^{ch} + P_{i,t}^{dch}\right) - P_{i,t}^L = \sum_{j \in \Omega_\ell^i} P_{ij,t} : \lambda_{i,t}^P \tag{6}$$

$$Q_{i,t}^g + Q_{i,t}^{LS} + Q_{i,t}^W - Q_{i,t}^L = \sum_{j \in \Omega_\ell^i} Q_{ij,t} : \lambda_{i,t}^q \tag{7}$$

where $P_{i,t}^L$ is the electric demand on bus i at time t. $Q_{i,t}^W$ is the reactive power generated by the wind turbine connected to bus i at time t.

D. Thermal Power Plant Constraints

The maximum and minimum values of the active and reactive fossil power plants and their ramp up/down rate constraints are as follows [41], [35]:

$$P_{i,t}^{g,\min} \le P_{i,t}^g \le P_{i,t}^{g,\max} \tag{8}$$

$$Q_{i,t}^{g,\min} \le Q_{i,t}^g \le Q_{i,t}^{g,\max} \tag{9}$$

$$P_{i,t+1}^g - P_{i,t}^g \le RU_g \tag{10}$$

$$P_{i,t-1}^g - P_{i,t}^g \le RD_g \tag{11}$$

E. Load Shedding Constraints

$$0 \le P_{i,t}^{LS} \le P_{i,t}^L \tag{12}$$

$$0 \le Q_{i,t}^{LS} \le Q_{i,t}^L \tag{13}$$

F. ESS and DG Constraints

The constraints related to energy storage systems (ESSs) are as follows [42]:

$$SOC_t = SOC_{t-1} + \left(P_t^{ch}\eta_{ch} - P_t^{dch}/\eta_{dch}\right)\Delta t \tag{14}$$

$$SOC_{\min} \le SOC_t \le SOC_{\max} \tag{15}$$

$$P_{\min}^{ch} \le P_t^{ch} \le P_{\max}^{ch} \tag{16}$$

$$P_{\min}^{dch} \le P_t^{dch} \le P_{\max}^{dch} \tag{17}$$

where SOC_t is the charge state of the ESS at time t.

The constraints related to the wind power plants are as follows:

$$P_{i,t}^{WC} = w_t\Lambda_i^w - P_{i,t}^W \tag{18}$$

$$0 \le P_{i,t}^W \le w_t\Lambda_i^w \tag{19}$$

Similarly, the solar power plant constraints can be defined as:

$$P_{i,t}^{SC} = s_t\Lambda_i^S - P_{i,t}^S \tag{20}$$

$$0 \le P_{i,t}^S \le s_t\Lambda_i^S \tag{21}$$

where $P_{i,t}^s$ and $P_{i,t}^{sc}$ are the solar generation and solar curtailment in bus i at time t , respectively. S_t is the

solar availability at time t, and Δ_i^s the solar power plant capacity in bus i.

2.4. Demand response program

A time-value-based demand-shifting strategy was used to reduce the peak load and shift this value to other mid-peak and low-demand hours [43]. According to this strategy, the electrical power consumption at bus i and time t in the presence of the demand response scheme ($P_{i,t}^L$) is calculated as the sum of the base load ($P_{i,t}^{L0}$) and the decision variable of the demand response ($DR_{i,t}$). if $DR_{i,t}>0$, the active power demand of the ith bus will increase at hour t and valley filling will occur. Similarly, If $DR_{i,t}<0$, the active power demand of the ith bus will decreases at hour t; hence peak shaving occurs. Another possible state is when $DR_{i,t}$ is zero; in this case, no demand response program occurs. The algebraic sum of the load reduction and increase in each bus should be zero. The maximum and minimum load response values were also determined using Equation (24). In this method, only the active power changes are considered. In this study, the effect of demand response on reactive power is also considered, so that the power factor before the load response and the active power after the load response is used to calculate the new reactive power. It is assumed that before and after the demand response, the power factor of the loads has a constant value. The formulae for the above expressions are as follows.

$$P_{i,t}^{L} = P_{i,t}^{L0} + DR_{i,t}; \quad \forall i \tag{22}$$

$$\sum_{t=1}^{24} DR_{i,t} = 1; \quad \forall i \tag{23}$$

$$-\alpha \cdot P_{i,t}^{L0} \le DR_{i,t} \le \alpha \cdot P_{i,t}^{L0}; \quad \forall i \tag{24}$$

$$\tan\left(\theta_{i,t}\right) = \frac{Q_{i,t}^{L0}}{P_{i,t}^{L0}} \tag{25}$$

$$Q_{i,t}^{L} = \tan\left(\theta_{i,t}\right) P_{i,t}^{L} \tag{26}$$

3. Case studies and data

The proposed DR program was tested on a modified IEEE 24-bus system [35], as shown in Figure 4, where 100 and 50 MW PV solar power plants were added to buses 3 and 23, respectively. In addition to thermal power plants, this structure consists of three wind power plants (With a capacity of 200, 150, and 100 in 8, 19, and 21 basses) and two battery energy storage systems (BESS). These two BESSs, with capacities of 200 and 100, are located in buses 19 and 21, respectively. The charging and discharging efficiencies of the BESS are 95% and 90%, respectively, and the minimum and maximum charge/discharge rates are considered to be zero and 20% of the maximum storage capacity, respectively. In addition, the minimum state of charge (SOC0) was 20% of its maximum capacity.

Because of the nonlinear problem, GAMS software by nonlinear programming (NLP) was used to solve the problem. In this structure, the characteristics of the power transmission lines, such as resistance, reactance, susceptance, and capacity, are shown in Table 1. The fuel cost factor (b_g), ramp up/down rate (RU_g, RD_g), and minimum and maximum limits of active and reactive power ($P_i^{g,min}$, $P_i^{g,max}$, $Q_i^{g,min}$, $Q_i^{g,max}$) for each thermal generation unit are listed in table 2. The base power used was 100 MVA. Bus 13 of the test system is considered a slack bus ($1<0^{\circ}$) and the minimum and maximum per-unit values of the voltage range in the buses are 0.9 and 1.1. The real and reactive power loads of bus i are listed in Table 3. By using the amount of active and reactive power, it is possible to calculate the power factor of the loads. The power output variation of solar and wind plants (hypothetical) and demand changes (anticipated in Section 2.1) during the day are shown in Figure 5.

In [44], mobile battery storage was used to evaluate the cost of curtailed wind energy, and the evaluation result of VOLW reached a range of 150 - 249 $/MWh. In the present study, the VOLW value was 200. In [45], the changes in the VOLS value have been between 33.8 and 112.8 $/MWh, where the value of 100 is considered.

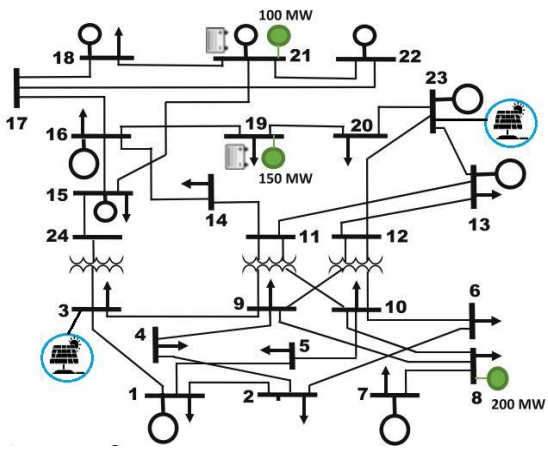

Figure 4. A modified IEEE 24-bus system

Table 1. characteristics of power transmission lines [35]

line	r	x	b	Limit
1 .2	0.0026	0.0139	0.4611	175
1 .3	0.0546	0.2112	0.0572	175
1 .5	0.0218	0.0845	0.0229	175
2 .4	0.0328	0.1267	0.0343	175
2 .6	0.0497	0.192	0.052	175
3 .9	0.0308	0.119	0.0322	175
3 .24	0.0023	0.0839	0	400
4 .9	0.0268	0.1037	0.0281	175
5 .10	0.0228	0.0883	0.0239	175
6 .10	0.0139	0.0605	2.459	175
7 .8	0.0159	0.0614	0.0166	175
8 .9	0.0427	0.1651	0.0447	175
8 .10	0.0427	0.1651	0.0447	175
9 .11	0.0023	0.0839	0	400
9 .12	0.0023	0.0839	0	400
10.11	0.0023	0.0839	0	400
10.12	0.0023	0.0839	0	400
11.13	0.0061	0.0476	0.0999	500
11.14	0.0054	0.0418	0.0879	500
12.13	0.0061	0.0476	0.0999	500
12.23	0.0124	0.0966	0.203	500

Table 2. characteristics of thermal generation unit [35]

bus	Pmax (MW)	Pmin (MW)	b ($/MW)	Qmax (MVAR)	Qmin (MVAR)
1	152	30.4	13.32	192	-50
2	152	30.4	13.32	192	-50
7	350	75	20.7	300	0
13	591	206.85	20.93	591	0
15	215	66.25	21	215	-100
16	155	54.25	10.52	155	-50
18	400	100	5.47	400	-50
21	400	100	5.47	400	-50
22	300	0	0	300	-60
23	360	248.5	10.52	310	-125

Table 3. The value of active and reactive loads of each bus [35]

bus	P (MW)	Q (MVAR)
1	108	22
2	97	20
3	180	37
4	74	15
5	71	14
6	136	28
7	125	25
8	171	35
9	175	36
10	195	40
13	265	54
14	194	39
15	317	64
16	100	20
18	333	68
19	181	37
20	128	26

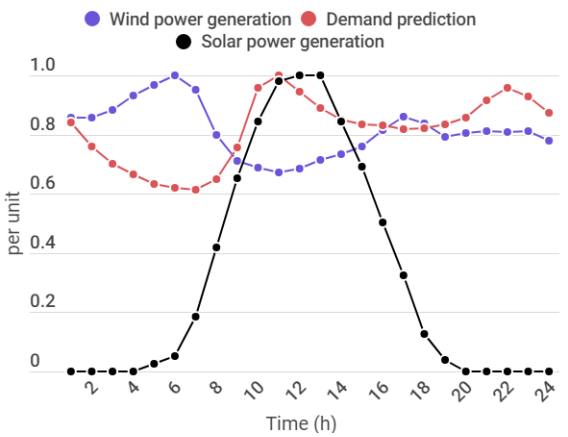

Figure 5. Daily power generation of solar and wind plants and load demand curves

To extract the best optimal solution from a multi-objective OPF problem, a technique for order preference by similarity to ideal solution (TOPSIS) is implemented to select the best solution. The steps of this method include the calculation of the normalized matrix, the weighted normalized matrix, the best and worst ideal value for each of the objective functions, the Euclidean distance between each of the weighted normalized and ideal solutions, and finally scoring each state. The details of this method are mentioned in [46].

4. Results & discussion

These results were implemented with an Intel Corei7, 2.2 GHz CPU, 6 GB of RAM, and a 500 GB hard disc computer. This problem was modeled in the Generic Algebraic Modeling System (GAMS) environment and solved using CONOPT as an NLP solver. This section is divided into two parts: validation and optimization results.

4.1 Validation

Table 4 presents the effect of the demand response using the proposed method compared with those reported by Soroudi [35] (without DR) and Jabari et al. [23] (only active power participated in the DR). A maximum DR rate of 20% was considered. The total cost was reduced by considering the DR program. If DR occurs in the reactive power in addition to the active power, a reduction in the peak and an increase in the valley will occur for the reactive power. Figure 6 and 7 illustrate this explanation. In this study, the cost of the reactive power is considered fixed (as described in Section 2.2); however, shifting the required reactive power during the peak load curve to its low load also reduces the cost of reactive power generation.

Table 4. Comparison of total cost and peak reduction

OFs \ Cases		Ref [35]	Ref [23]	Proposed method
TC ($\times 10^3$\$)		442.3	415.6	415.6
Active load (MW)	Peak	2850	2455	2455
	Valley	1750	2100	2100
Rective load (MVAR)	Peak	580	580	500
	Valley	356	356	427

(TC=Total cost, VDF=Voltage Deviation Function, PR=peak reduction)

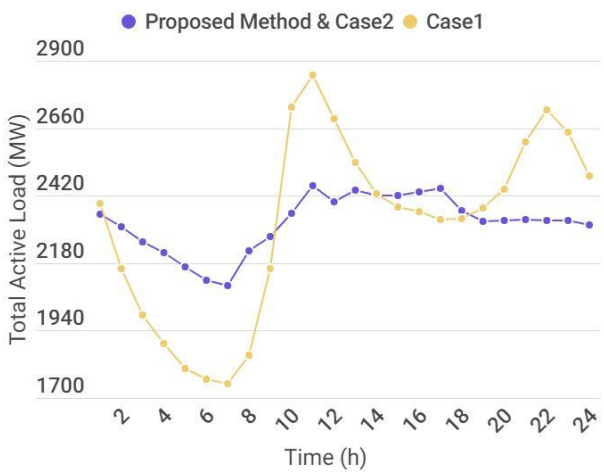

Figure 6. Total active load profile

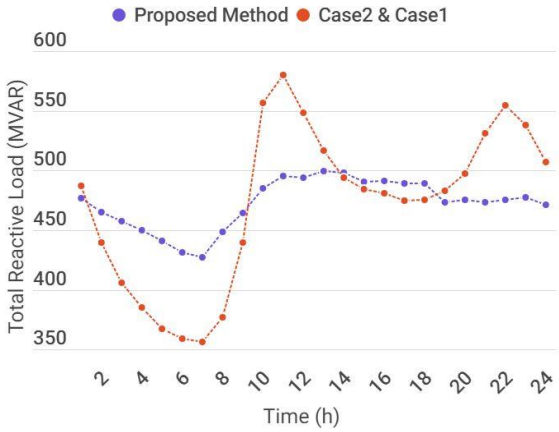

Figure 7. Total reactive load profile

4.2 Optimization results

Table 5 presents the results of the optimization. According to this table, demand response reduces the cost of the entire system, reduces the peak load, increases the load valley, and improves the load factor of the power grid. For example, with a 20% demand response, a 13.85% reduction in the peak load and a 20% increase in the valley load were achieved. Shifting the load consumption during peak hours to valley hours reduces the cost for the consumer, eliminates the need for expensive power plants during peak load, and can cancel or postpone the construction of new power plants.

To highlight the advantages of demand response, Figure 8 shows the total electrical load profile before and after the demand response. The percentages of load participation in the demand response were considered to be 5, 10, 15, 20, and 25%, respectively. It can be seen that with increasing demand response, the peak value decreases significantly, the valley value increases, and the load curve becomes more levelized. Increasing the demand response rate of the load may cause time displacement of the peak load, and thus, its amount should be controlled.

Figure 9 shows the hourly dispatch of the ESS before and after the demand response. By increasing the participation of loads in the demand response, the number of times and amount of charging and discharging cycles of the ESS decreases. Because the number of charging and discharging cycles is inversely related to the life of the ESS, the demand response increases the life of the energy storage equipment.

Table 5. Results of multi-objective OPF

	Proposed DR					
DR Percent	NA	5	10	15	20	25
TC ($\times 10^3$\$)	442.3	426.4	420.9	417.5	415.6	414.8
TVD (p.u.)	25.28	24.87	25.76	25.81	26.14	26.31
PR (%)	0.00	5.00	0.06	11.58	13.85	13.87
Peak (MW)	2850	2708	2592	2520	2455	2454
Valley (MW)	1750	1838	1925	2012	2100	2100
Load Factor	0.815	0.858	0.904	0.928	0.945	0.949
Peak (MVAR)	580	551	523	509	500	449
Valley (MVAR)	356	374	391	410	427	445
Peak to Valley (MVAR)	224	177	131	100	73	54

(TC=Total cost, VDF=Voltage Deviation Function, PR=peak reduction, NA=not applied)

The voltage level of the load and generation at each bus is very important for supply quality. Figure 10 shows the voltage profile variation at bus 6 in the three states without DR, 10% DR, and 20% DR. As shown, with the increase in DR, the variation in the bus voltage is more limited. The voltage profile of the IEEE 24-bus test system is shown in Figure 11, from which it can be seen that the voltages at buses 1, 2, 4, and 7 are near the considered specified limit of -10% because these buses are far away from the main grid supply points (thermal, solar, and wind power plants) or have a high generation cost. In contrast, buses 20, 22, and 23 have a maximum voltage limit (+10%) because they have renewable energy sources, or the power plant connected to them has a low production cost.

The TOPSIS method was used to compare different states of the demand response. Because of the importance of economic issues and peak shaving, the weighting coefficients of the cost, total deviation voltage (TDV), and peak reduction (PR) functions are 0.35, 0.3, and 0.35, respectively. As presented in Table 6, the multi-objective optimization analysis with TOPSIS shows that the most optimal state occurs when the demand response is 20%, which indicates that an excessive increase in the demand response requirement shifts the peak load to another time.

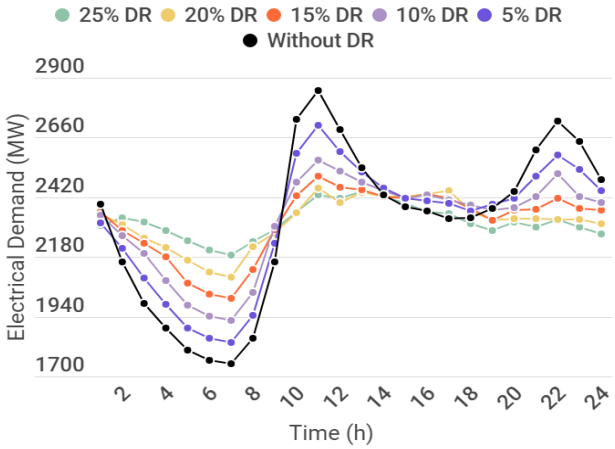

Figure 8. Electrical load profile before and after DR

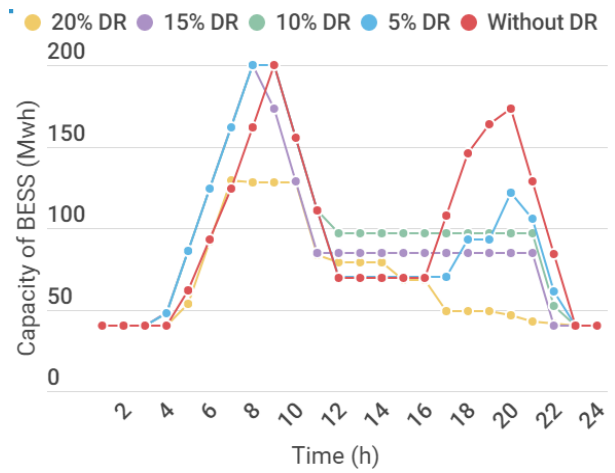

Figure 9. SOC of BESS at bus 19

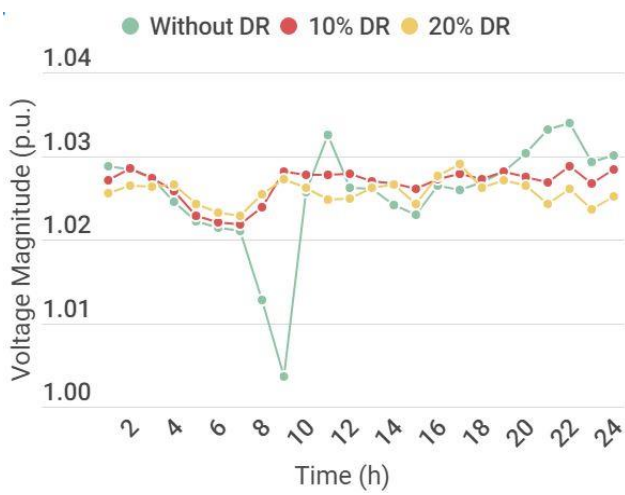

Figure 10. Voltage profile at bus 6

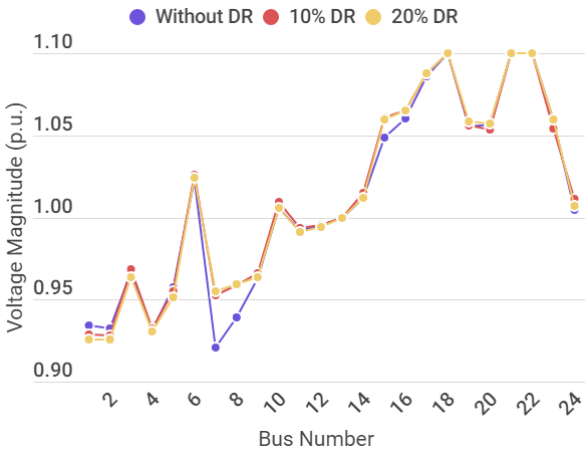

Figure 11. Voltage profile of the IEEE 24-bus system

Table 6. Results of the TOPSIS method

OFs / Weight / DR%	TC	TDV	PR	P_i	Rank
	0.35	0.3	0.35		
25	0.140	0.125	0.208	0.968	2
20	0.140	0.125	0.208	0.972	1
15	0.141	0.123	0.174	0.834	3
10	0.142	0.123	0.001	0.036	5
5	0.144	0.119	0.075	0.362	4
0	0.149	0.120	0.000	0.023	6

5. Conclusions

In this study, the DSM-based AC optimal power flow was investigated by a multi-objective problem constructed with some cost functions using the weighted sum method. In the proposed method, both active and reactive powers were applied to the demand response problem. In addition to reducing the peak load, the total cost and total voltage deviation were considered; thus, the problem of moving the peak load was minimized. In addition to using the deep learning method to predict the load based on the previous data, the accuracy of the response increased. The TOPSIS method is used to determine the optimal point in multi-objective optimization. The optimization results show that the proposed demand response (20%) not only achieved peak reduction and valley filling but also minimized the Total Voltage Deviation and system cost. Reducing the demand-supply gap, decreasing the charge and discharge of energy storage systems, and increasing the quality of service are other benefits of the proposed demand response programs.

Considering the space of the smart network, it was assumed that all the loads were involved in the Demand response problem, and in future research, some of the loads can be considered as elastic (participating in DR) and another part as inelastic.

Nomenclature

Subscripts

ADMM	Alternating direction method of multipliers
AI	Artificial Intelligence
BESS	Battery Energy Storage System
DERs	Distributed Energy Resources
DMPC	Distributed Model Predictive Control
DR	Demand Response
DSM	Demand side management
EEC	Energy efficiency and conservation
ESS	Energy Storage System
IBDR	Incentive-based demand response
LSE	Load serving entities
LSTM	Long short-term memory
NLP	Non-Linear Programming
OPF	Optimal power flow
PBDR	Price-based demand response
PR	Peak reduction
PV	Photovoltaic
SG	Smart Grid
SOC	State of charge
TDV	Total deviation voltage
VDF	Voltage Deviation Function

Indices and Sets

ch/dch	Index denotes the charge/discharge state of ESS.
g	Index denotes the thermal generation units.
i,j	Index denotes the network buses.
t	Time indicator
w	Index denotes the wind turbine units.
Ω^i_t	Set of all buses connected to bus i

Parameters and Variables

b_g	fuel cost coefficient of active power

	generation at unit g ($/MW)
b	Susceptance of transmission line
c_g	fuel cost coefficient of reactive power generation at unit g ($/MW)
$P_{ch}^{max}/P_{dch}^{max}$	maximum charging and discharging limits (MW)
$P_{ch}^{min}/P_{dch}^{min}$	minimum charging and discharging limits (MW)
$P_{i,t}^{ch}/ P_{i,t}^{dch}$	Charging/discharging power of ESS (MW)
$P_{i,t}^{L} / P_{i,t}^{L0}$	Active power consumption at bus i and time t after/before demand response (MW)
$P_{i,t}^{LS}$	Active Load shedding in bus i at time t (MW)
$P_{i,t}^{WC}/ P_{i,t}^{SC}$	Wind/solar curtailment in bus i at time t (MW)
$P_{i,t}^{S}$	Solar power plant generation in bus i at time t (MW)
$P_{ij,t} / Q_{ij,t}$	Active/reactive power flow from bus i to bus j (MW / MVAR)
$P_i^{g,min}/P_i^{g,max}$	minimum and maximum limits of active power (MW)
P_{load}^{new}	Active Load after demand response (MW)
P_{load}^{old}	Active Load before demand response (MW)
$Q_i^{g,min}/Q_i^{g,max}$	minimum and maximum limits of reactive power (MVAR)
$Q_{i,t}^{L} / Q_{i,t}^{L0}$	Reactive power consumption at bus i and time t after/before demand response (MVAR)
$Q_{i,t}^{LS}$	Reactive Load shedding in bus i at time t (MVAR)
$Q_{i,t}^{W}$	wind turbine reactive power generation (MVAR)
RU_g/RD_g	ramp up/down rate (MW/h)
$S_{ij,t}$	Complex power flow from bus i to j (MVA)
S_t	solar availability in time t (p.u)
SOC_t	State of charge of ESS at time t (MWh)
V_i	Bus voltage magnitude at the bus i (p.u)
$VOLL$	value of loss of load ($/MWh)
$VOLW$	value of loss of wind ($/MWh)
$VOLS$	value of loss of solar ($/MWh)
w_t	wind availability in time t (p.u)
$Z_{ij}<\theta_{ij}$	impedance of transmission line i to j (p.u<deg)
Λ_t^S / Λ_t^w	Solar/Wind availability at time t (p.u)
λ_i	Locational marginal price in bus i ($/MWh).
δ_i	Bus voltage angle at the bus i (deg)
η_{ch} / η_{dch}	Charge/discharge efficiency of ESS

References

1. Hussain, S., et al., Multi-level energy management systems toward a smarter grid: A review. IEEE Access, 2021. 9: p. 71994-72016.
2. Nasir, T., et al., Recent challenges and methodologies in smart grid demand side management: State-of-the-art literature review. Mathematical Problems in Engineering, 2021. 2021.
3. Kabir, E., et al., Solar energy: Potential and future prospects. Renewable and Sustainable Energy Reviews, 2018. 82: p. 894-900.
4. Holm-Nielsen, J.B. and E.A. Ehimen, Biomass supply chains for bioenergy and biorefining. 2016: Woodhead Publishing.
5. Nazir, M.S., et al., Environmental impact and pollution-related challenges of renewable wind energy paradigm – A review. Science of The Total Environment, 2019. 683: p. 436-444.
6. Zhao, L.-C., et al., Magnetic coupling and flextensional amplification mechanisms for high-robustness ambient wind energy harvesting. Energy Conversion and Management, 2019. 201: p. 112166.
7. Olabi, A. and M. Abdelkareem, Energy storage systems towards 2050. 2021, Elsevier. p. 119634.
8. Mbachu, V.M., et al., An Economic Based Analysis of Fossil Fuel Powered Generator and Solar Photovoltaic System as Complementary Electricity Source for a University Student's Room. Journal of

Solar Energy Research, 2022. 7(4): p. 1159-1173.
9. Jalili Jamshidian, F., S. Gorjian, and M. Shafiee Far, An Overview of Solar Thermal Power Generation Systems. Journal of Solar Energy Research, 2018. 3(4): p. 301-312.
10. Logenthiran, T., D. Srinivasan, and T.Z. Shun, Demand side management in smart grid using heuristic optimization. IEEE transactions on smart grid, 2012. 3(3): p. 1244-1252.
11. Setlhaolo, D. and X. Xia, Combined residential demand side management strategies with coordination and economic analysis. International Journal of Electrical Power & Energy Systems, 2016. 79: p. 150-160.
12. Vardakas, J.S., N. Zorba, and C.V. Verikoukis, A survey on demand response programs in smart grids: Pricing methods and optimization algorithms. IEEE Communications Surveys & Tutorials, 2014. 17(1): p. 152-178.
13. Bhattacharya, S., K. Kar, and J.H. Chow. Optimal precooling of thermostatic loads under time-varying electricity prices. in 2017 American Control Conference (ACC). 2017. IEEE.
14. Bari, A., et al., Challenges in the smart grid applications: an overview. International Journal of Distributed Sensor Networks, 2014. 10(2): p. 974682.
15. Xia, X., D. Setlhaolo, and J. Zhang. Residential demand response strategies for South Africa. in IEEE Power and Energy Society Conference and Exposition in Africa: Intelligent Grid Integration of Renewable Energy Resources (PowerAfrica). 2012. IEEE.
16. Rahmani-andebili, M., Modeling nonlinear incentive-based and price-based demand response programs and implementing on real power markets. Electric Power Systems Research, 2016. 132: p. 115-124.
17. Ahmadipour, M., et al., Optimal load shedding scheme using grasshopper optimization algorithm for islanded power system with distributed energy resources. Ain Shams Engineering Journal, 2023. 14(1): p. 101835.
18. Louca, R. and E. Bitar, Robust AC optimal power flow. IEEE Transactions on Power Systems, 2018. 34(3): p. 1669-1681.
19. Taylor, J.A., Convex optimization of power systems. 2015: Cambridge University Press.
20. Chatzivasileiadis, S., Lecture notes on optimal power flow (OPF). arXiv preprint arXiv:1811.00943, 2018.
21. Li, B., et al., Generalized linear‐constrained optimal power flow for distribution networks. IET Generation, Transmission & Distribution, 2023.
22. Abdi, H., S.D. Beigvand, and M. La Scala, A review of optimal power flow studies applied to smart grids and microgrids. Renewable and Sustainable Energy Reviews, 2017. 71: p. 742-766.
23. Jabari, F., M. Mohammadpourfard, and B. Mohammadi-Ivatloo, AC Optimal Power Flow Incorporating Demand-Side Management Strategy, in Demand Response Application in Smart Grids. 2020, Springer. p. 147-165.
24. Haggi, H., et al., Risk-averse cooperative operation of PV and hydrogen systems in active distribution networks. IEEE Systems Journal, 2021. 16(3): p. 3972-3981.
25. Shi, Y., et al., Distributed model predictive control for joint coordination of demand response and optimal power flow with renewables in smart grid. Applied Energy, 2021. 290: p. 116701.
26. Yao, M., D.K. Molzahn, and J.L. Mathieu, An optimal power-flow approach to improve power system voltage stability using demand response. IEEE Transactions on Control of Network Systems, 2019. 6(3): p. 1015-1025.
27. Heidari Yazdi, S.S., et al., Over-voltage regulation of distribution networks by coordinated operation of PV inverters and demand side management program. 2022.
28. Merrad, Y., et al., Fully Decentralized, Cost-Effective Energy Demand Response Management System with a Smart Contracts-Based Optimal Power Flow Solution for Smart Grids. Energies, 2022. 15(12): p. 4461.
29. Ghalehkhondabi, I., et al., An overview of energy demand forecasting methods published in 2005–2015. Energy Systems, 2017. 8(2): p. 411-447.
30. Nti, I.K., et al., Electricity load forecasting: a systematic review. Journal of Electrical Systems and Information Technology, 2020. 7(1): p. 13.

31. Bouktif, S., et al., Optimal deep learning lstm model for electric load forecasting using feature selection and genetic algorithm: Comparison with machine learning approaches. Energies, 2018. 11(7): p. 1636.
32. Dargan, S., et al., A survey of deep learning and its applications: a new paradigm to machine learning. Archives of Computational Methods in Engineering, 2020. 27(4): p. 1071-1092.
33. Alzubi, J., A. Nayyar, and A. Kumar. Machine learning from theory to algorithms: an overview. in Journal of physics: conference series. 2018. IOP Publishing.
34. https://www.transpower.co.nz/system-operator/operational-information/load-graphs#download. Available from: "https://www.transpower.co.nz/system-operator/operational-information/load-graphs#download.
35. Soroudi, A., Energy Storage Systems: Power system optimization modeling in GAMS. Vol. 78. 2017: Springer.
36. Wolgast, T., S. Ferenz, and A. Nieße, Reactive power markets: A review. IEEE Access, 2022.
37. Halbhavi, S., S. Karki, and S. Kulkarni, Reactive Power Pricing Framework Problems and a proposal for a competitive market. International Journal of Innovations in Engineering and Technology, 2012. 1(2): p. 22-27.
38. Deng, Z., M.D. Rotaru, and J.K. Sykulski. A study of evolutionary based optimal power flow techniques. in 2016 51st International Universities Power Engineering Conference (UPEC). 2016. IEEE.
39. Aalami, H., M.P. Moghaddam, and G. Yousefi, Modeling and prioritizing demand response programs in power markets. Electric Power Systems Research, 2010. 80(4): p. 426-435.
40. Grigsby, L.L., Electric power engineering handbook. 2006: CRC Press LLC, London.
41. Ghaffarzadeh, N. and H. Faramarzi, Optimal Solar plant placement using holomorphic embedded power Flow Considering the clustering technique in uncertainty analysis. Journal of Solar Energy Research, 2022. 7(1): p. 997-1007.
42. Bozorgavari, S.A., et al., Robust planning of distributed battery energy storage systems in flexible smart distribution networks: A comprehensive study. Renewable and Sustainable Energy Reviews, 2020. 123: p. 109739.
43. Jabari, F., M. Mohammadpourfard, and B. Mohammadi-Ivatloo, Implementation of Demand Response Programs on Unit Commitment Problem, in Demand Response Application in Smart Grids. 2020, Springer. p. 37-54.
44. Siddique, M.B. and J. Thakur, Assessment of curtailed wind energy potential for off-grid applications through mobile battery storage. Energy, 2020. 201: p. 117601.
45. Bolinger, M., J. Seel, and D. Robson, Utility-scale solar: Empirical trends in project technology, cost, performance, and PPA pricing in the United States–2019 Edition. 2019.
46. Elattar, E.E., et al., Optimal power flow with emerged technologies of voltage source converter stations in meshed power systems. IEEE Access, 2020. 8: p. 166963-166979.